Opto-Electronic Engineering

Article

2017, Vol 44, Issue 2

Subwavelength filter and sensor design based on end-coupled composited ring-groove resonator

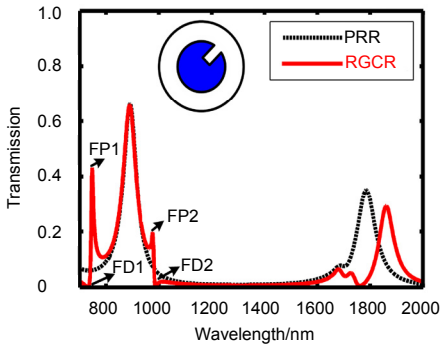

Kunhua Wen*, Yihua Hu, Li Chen, Jinyun Zhou, Miao He, Liang Lei and Ziming Meng

School of Physics and Optoelectronic Engineering, Guangdong University of Technology, Guangzhou 510006, China

Abstract: A plasmonic filter and sensor is designed based on an end-coupled ring-groove composited resonator (RGCR). According to the magnetic field distributions of the resonance modes, a horizontal or vertical groove is added to the perfect ring resonator, and the transmission peaks for the 1st and the 2nd modes can be linearly changed by the length of the groove. In this case, the proposed structure can act as an on-chip optical filter with flexible wavelength manipulation. When the groove is rotated with an angle of $\pi/4$, Fano resonance arises due to the mode interference. Dual asymmetric sharp transmission peaks are achieved around the wavelength of the former 2nd resonance mode. High figure of merit and high sensitivity are obtained for the structure, and it is believed that the device can find widely applications in the biochemistry sensing area. The corresponding spectra and the propagation characteristics are numerically investigated by using the finite-difference time-domain method.

Keywords: plasmonic filter; sensor; Fano resonance

DOI: 10.3969/j.issn.1003-501X.2017.02.007 **Citation:** *Opto-Elec Eng*, 2017, **44**(2): 192−197

1 Introduction

Recently, high integrated photonic circuits have been widely developed by taking advantages of surface plasmon polaritons (SPPs) [1-4], which are considered as one of most promising ways to overcome the diffraction limit of lightwave. In particular, various plasmonic metal-insulator-metal (MIM) waveguide structures [5-6], which show great potentials in the optical communication due to the advantages of easy fabrication and strong light confinement, have been proposed and demonstrated, such as MZI-based device[7], Y-shaped combiners [8], couplers [9-10], and optical waveguides [11-12]. As the important unit in the optical signal processing module [13-14], MIM-based optical filter has also received considerable interest. For example, plasmonic band-stopped filters were achieved in the MIM structures that were constructed by periodic insulators or grooves [15-24]. Side-coupled or end-coupled slot cavities, which acted as Fabry–Pérot (FP) resonators, were also proposed to obtain multiple filtering channels [25-27]. For those traditional optical filters, one may mainly concern on the manipulations of the center wavelength and the spectral line shape. Usually, the resonance wavelength has a linearly relationship with the length of the resonator, while symmetric spectrum with narrow line width is preferred for the filter. However, Fano resonance, which is attributed to the modes interactions, possesses asymmetric sharp transmission peaks [28]. Distinguished from the traditional filtering characteristics, the structures with Fano resonance will be appropriate for the sensing due to the high figure of merits (FOM) and the high sensitivity. Asymmetric spectral line shapes were achieved by using the MIM structures with two parallel grooves or two side-coupled slot cavities [29-30]. Fano resonance was also investigated by employing the T-shaped resonators [31-32].

In this paper, an optical filter based on a subwavelength end-coupled ring-groove composited resonator (RGCR) is firstly proposed and investigated. The position of the groove is the key factor to manipulate the 1st or 2nd resonance mode, and the wavelength of the expected mode can be linearly changed by the length of the groove. In this case, the proposed structure can act as an on-chip

Received 05 November 2016; accepted 10 December 2016
* E-mail: khwen@gdut.edu.cn

optical filter. When the groove is rotated $\pi/4$, Fano resonance arises due to the interference between the dark mode and the bright mode. Dual asymmetric-sharp transmission peaks are achieved with high FOM and high sensitivity. Finite-difference time-domain (FDTD) method with perfectly matched layer (PML) boundary conditions is used to investigate the performance of the MIM RGCR structure.

2 Theories and analyses

Fig. 1 shows the schematic diagram of the proposed MIM structure, and the metal and insulator are assumed as silver and air, respectively. The RGCR is placed between the input and output MIM waveguides with coupling distances of s_1 and s_2, respectively. The angle φ between the normal line and the groove is used to identify the position of the groove. It is well known that the perfect ring (PR) structure can be regarded as a FP resonator, and the resonance phase condition is given as:

$$k\mathrm{Re}(n_{\mathrm{eff}})L_{\mathrm{eff}} = 2m\pi, \quad m = 1, 2, 3, \cdots, \tag{1}$$

where $L_{\mathrm{eff}} = \pi(R+r)$ is the equivalent resonant length, r and R are the inner radius and the outer radius, respectively, m is an integer that stands for the resonance mode, $k = 2\pi/\lambda$ is the wave-vector in free space, and $\mathrm{Re}(n_{\mathrm{eff}})$ is the real part of the effective refractive index n_{eff} which can be calculated from the dispersion equation in the waveguide given by [33]:

$$\varepsilon_{\mathrm{a}} k_{\mathrm{s}} + \varepsilon_{\mathrm{s}} k_{\mathrm{a}} \tanh(-\mathrm{j}k_{\mathrm{a}}W/2) = 0, \tag{2}$$

where $k_{\mathrm{a,s}} = \sqrt{\varepsilon_{\mathrm{a,s}} k_0^{\,2} - \beta^2}$ is the transverse propagation constants in air and silver, respectively, W is the width of the waveguide, $\beta = k_0 n_{\mathrm{eff}}$ is the propagation constant, and ε_{a} and ε_{s} are the permittivity of air and silver, respectively.

According to equation (1) for those FP filters, it can be concluded that the center wavelengths for the resonance modes are mainly determined by the effective length of the resonator. We only consider the 1st and the 2nd resonance modes for better analysis on the mechanism of wavelength manipulation by adding the groove. In the following simulations, the width of the MIM waveguide is W=50 nm, the inner and outer radii are r=170 nm and R=220 nm, respectively, the coupling distances are s_1=5 nm and s_2=10 nm, and the optical constants of silver are referred to the experimental data in Ref. [34]. In this case, the transmission spectrum of the PR resonator based on FDTD method is shown in Fig. 2(a). Obviously, two transmission peaks with high transmittance are obtained at the wavelengths of 890.6 nm and 1784.4 nm, respectively, and thus this kind of structure can be used as an optical filter. The center wavelengths for the two modes agree well with that analyzed in equation (1), i.e., the ratio of the wavelengths for the 1st and 2nd modes are 2: 1. According to equation (1), it can be also estimated that the wavelengths for all the modes can be changed proportionately by the length of the resonator. Therefore, it is interested to explore the method to only manipulate the expected mode.

The magnetic field intensities for both modes are also shown in Fig. 2(a), based on that we can design the position of the groove. Specifically, when the groove locates at the anti-node of magnetic field, SPPs are captured into the groove, and then the resonance wavelengths are changed by the groove. On the contrary, when the groove locates at the node, the corresponding SPP mode is not affected by the groove. Therefore, the groove is firstly placed at the top of the PR (i.e. φ=0°), where is the anti-node and the node for the 2nd and the 1st modes, re-

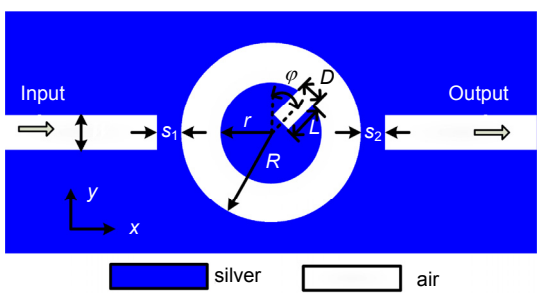

Fig. 1 Schematic diagram of the proposed plasmonic RGCR structure.

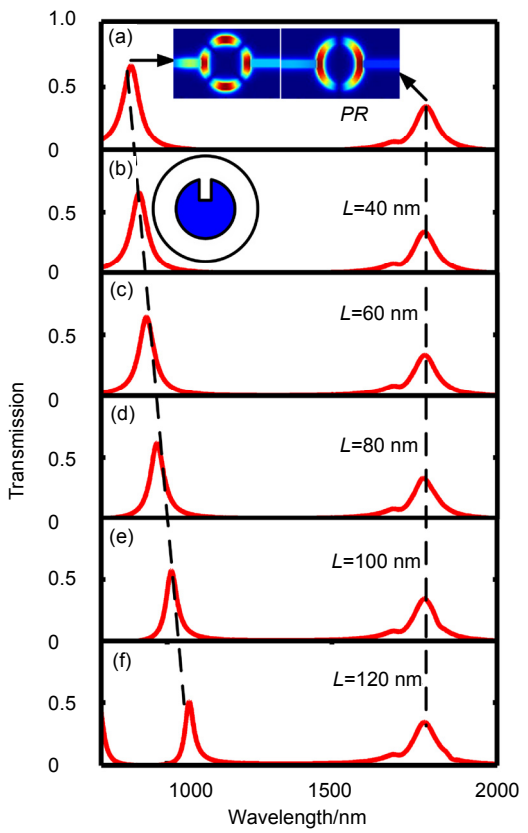

Fig. 2 Transmission spectra of (a) PR resonator, and (b)~(f) RGCR structures with φ=0°, and L=40, 60, 80, 100, and 120 nm, respectively.

spectively. Therefore, the wavelength for the 2nd mode can be manipulated by the groove, while the 1st mode keeps no change. By defining the width of the groove as D=30 nm firstly, the analysis results are further confirmed by the FDTD simulations. In the case of L=40, 60, 80, 100, and 120 nm, the wavelength for the 2nd mode is investigated to have a linear-proportional relationship with the length of the groove, and the corresponding wavelengths are 915.0, 937.2, 969.3, 1013.1 and 1066.8 nm in Figs. 2(b)~2(f), respectively, but the 1st mode always stays at the former wavelength of 1784.4 nm. The satisfactory filtering characteristics are also not affected in the RGCR structure. For example, high transmittance of ~0.5 and ~0.4 is always available for the 1st and the 2nd peaks. The quality factor Q factor is also used to evaluate the performance of the structure, and is expressed as:

$$Q = \frac{\lambda}{W_{\mathrm{FWHM}}}, \tag{3}$$

where W_{FWHM} is the full width at half maximum at the center resonance wavelength. The Q factors for the 2nd and the 1st resonance peaks are 14.2 and 21.5 in Fig. 2(a), 15.3 and 20.7 in Fig. 2(b), 16.9 and 20.7 in Fig. 2(c), 19.5 and 20.7 in Fig. 2(d), 24.4 and 20.7 in Fig. 2(e), and 32.3 and 20.7 in Fig. 2(f), respectively.

In addition, the groove is placed in the horizontal position, i.e., φ=90°, where the anti-nodes for both SPPs modes emerge, as shown in Fig. 2. According to the analysis above, it can be predicted that the center wavelengths for both modes are affected by the groove. The transmission spectra based on FDTD simulations are shown in Fig. 3. Compared to the spectrum of the PR resonator in Fig. 3(a), both transmission peaks have redshifts by adding a horizontal groove, whose lengths are 40, 60, 80, and 100 nm in Figs. 3(b)~3(e), respectively. The corresponding wavelengths and Q factors for the 1st and the 2nd modes are listed in Table 1. The Q factors for both transmission peaks are improved by increasing the length of the groove.

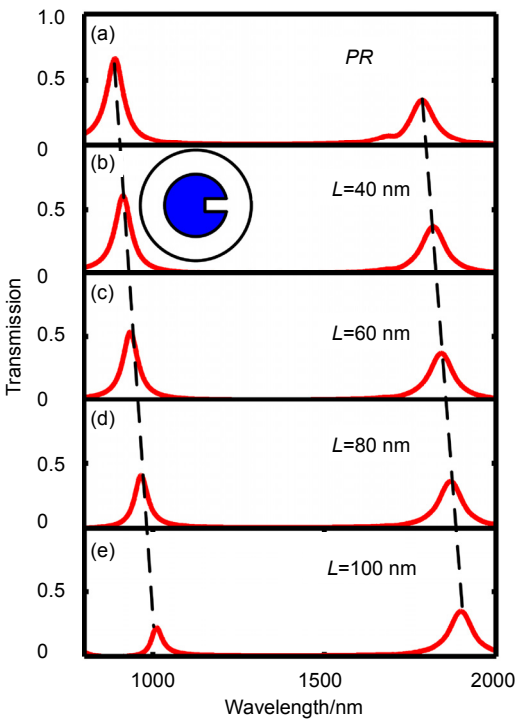

Fig. 3 Transmission spectra of (a) perfect ring resonator, (b)~(f) PR structure with φ=90°, and L=40, 60, 80, and 100 nm, respectively.

Furthermore, the groove is considered to be moved to the position with φ=45°, where is the anti-node for the 1st mode and the node for the 2nd mode, as illustrated in Fig. 2(a). The other parameters are the same as above during the simulations. Obviously, the transmission peak for the 1st mode of the RGCR structure has a relative redshift to the one of the PR resonator. Meanwhile, the peak wavelength for the 2nd mode in the RGCR structure is in accordance with that in the PR. Therefore, the band-pass filtering performance is not affected by the groove, since two channels are always obtained. However, one can flexibly manipulate the wavelengths of the expected modes through adjusting the position and the length of the groove. This proposed structure can provide more freedom to design the plasmoic filters.

Interestingly, in addition to the two symmetric peaks, it can be seen that Fano resonance with asymmetrical spectral profiles is also achieved due to the interference inside the RGCR structure. Two sharp Fano peaks (i.e. FP1 and FP2) with high transmittances of 0.43 and 0.20 occur at 747.2 and 975.8 nm, respectively. For FP1, the transmittance decreases rapidly at the left side of the sharp transmission peak, resulting in a transmission dip with ultra-low transmittance at 731.0 nm. Meanwhile, there is also the other transmission dip that emerges at 986.2 nm for FP2. The phase response and the delay time are analyzed in Fig. 4(b). Obviously, the phase has a shift during the Fano dip or the Fano peak. Since the delay time τ and the phase response satisfy the condition of $2\pi \cdot \partial\theta / \partial f$, it can be calculated that negative delay time and positive delay time are achieved at the dips and the peaks, respectively. The detailed results at the center wavelengths are as follows: -0.43 ps at FD1, 0.16 ps at FP1, -0.32 ps at FD2, and 0.12 ps at FP2, respectively. The dispersion d_ρ is determined by the time delay τ as d_ρ=dτ/dλ, and thus normal dispersion and abnormal dispersion are

Table 1 Wavelengths and Q factors with different lengths of the groove.

L/nm	1st SPP mode		2nd SPP mode	
	Wavelength/nm	Q	Wavelength/nm	Q
40	1818.0	15.5	915.7	22.2
60	1839.0	17.2	934.8	22.5
80	1868.0	20.3	966.7	23.1
100	1898.0	23.4	1010.0	24.5

available within the Fano peaks and dips, respectively. Therefore, on-chip slow light and fast light applications can be developed by using this proposed structure. More details about the SPPs propagation are investigated by using the magnetic field distributions in Fig. 5. Most of SPPs at the wavelengths of FD1 and FD2 are stopped by the RGCR structure, while the ones at FP1 and FP2 can pass through the output MIM waveguide.

To evaluate the performance of the RGCR structure that is used as a sensor, the sensitivity S and FOM are the two importance factors and are expressed as [35]

$$S = \frac{\mathrm{d}\lambda}{\mathrm{d}n(\lambda)}, \tag{4}$$

$$FOM^{*} = \left| \frac{\mathrm{d}T(\lambda)}{\mathrm{d}n(\lambda)} \frac{1}{T(\lambda)} \right|, \tag{5}$$

$$FOM = \max(FOM^{*}), \tag{6}$$

where $T(\lambda)$ is the transmittance at the specific wavelength, and $\mathrm{d}T(\lambda)/\mathrm{d}n(\lambda)$ is the transmittance variation induced by a refractive index change at the fixed wavelength. According to equation (5), we know that an ultra-low transmittance and a sharp increase induced by the index changes are preferred for obtaining a high FOM. When the length of the groove is defined as L=120, 140, and 160 nm, the transmission spectra are shown in Fig. 6(a). The wavelengths of the Fano peaks and dips increase linearly with the length of the groove, but the 2nd resonance mode always stay at 891 nm. It is further investigated that the Fano resonance is affected by the groove, and the 2nd SPP mode does not. Subsequently, the insulator inside the MIM waveguide is changed to be the one with the refractive index of n=1.0, 1.01, 1.03 and 1.05, respectively. By fixing L=100 nm, the transmission spectra, which are shown in Fig. 6(b), also present a redshift when increasing the refractive index almost linearly.

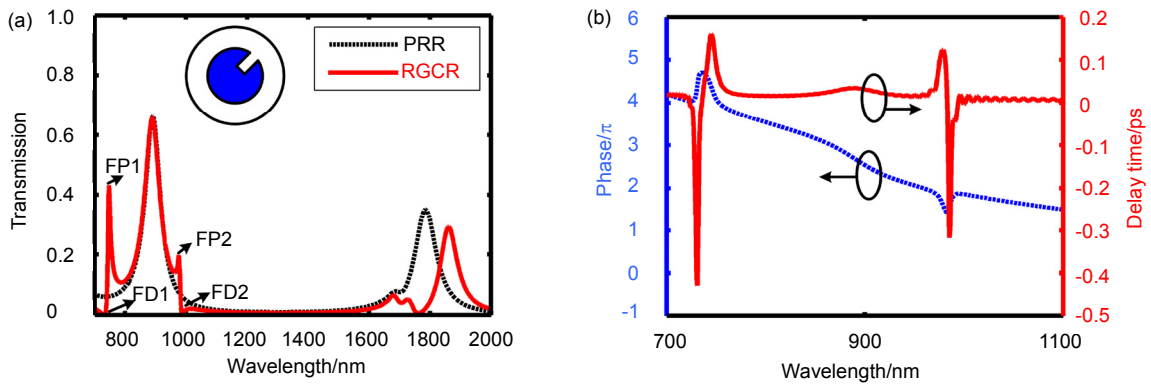

Fig. 4 (a) Transmission spectra of PR resonator and RGCR structure with φ=90° and L=100 nm, and (b) phase response and delay time.

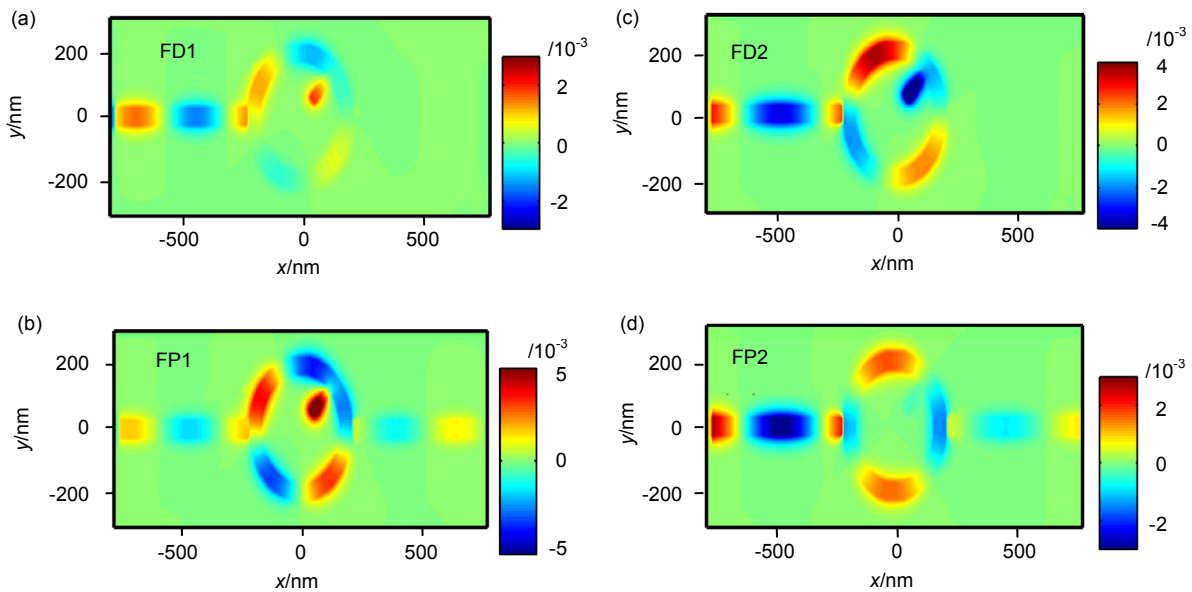

Fig. 5 Magnetic field distribution at the wavelengths of (a) FD1, (b) FP1, (c) FD2 and (d) FP2.

Based on equation (4), the sensitivity is derived as 728 nm/RIU and 970 nm/RIU for FP1 and FP2, respectively. As another evaluation criterion for the sensor, the FOM* variation with respect to the wavelength based on equation (5) is calculated in Fig. 6(c). High FOMs of 4.1×10^4 and 0.5×10^4 are achieved at the wavelengths of two Fano peaks, respectively. In this case, high performance of the RGCR structure that performs as a sensor is investigated, since high sensitivity and high FOM are obtained. One can design the on-chip biochemistry sensor by referring to this kind of RGCR structure.

3 Conclusions

In summary, a plasmonic RGCR filter and sensor based on FP and Fano resonance has been proposed and investigated by using MIM waveguides. As for a filter, two transmission peaks with high transmittance are achieved, and the wavelengths of the expected modes could be linearly manipulated by changing the position and the length of the groove, which makes the filter design more flexible and the resonance wavelength tunable. In addition, when the groove is with the angle of 45^o, Fano resonance with dual asymmetric sharp transmission peaks has also been achieved due to the mode interaction inside the RGCR structure. High sensitivity of 970 nm/RIU and high FOM of 4.1×10^4 are investigated by using the FDTD simulation. This kind of device may be widely applied in on-chip optical signal processing and bio-sensing area.

Acknowledgements

The work is supported by the National Natural Science Foundation of China under Grants (61405039) and (61475037), Science and Technology Planning Projects of Guangdong Province, China under Grant (2016A 020223013), the Natural Science Foundation of Guangdong Province, China, under Grant (2014A030310300), the Foundation for Distinguished Young Talents in Higher Education of Guangdong, China, under Grant (2014KQNCX066), Research Fund for the Doctoral Program of Higher Education of China under Grant (20134407 110008), Guangzhou Science and Technology Project of Guangdong Province, China under Grant (2016201604030027), and the Research Fund of Guangdong University of Technology under Grant (16ZK0041 , 13ZK0387).

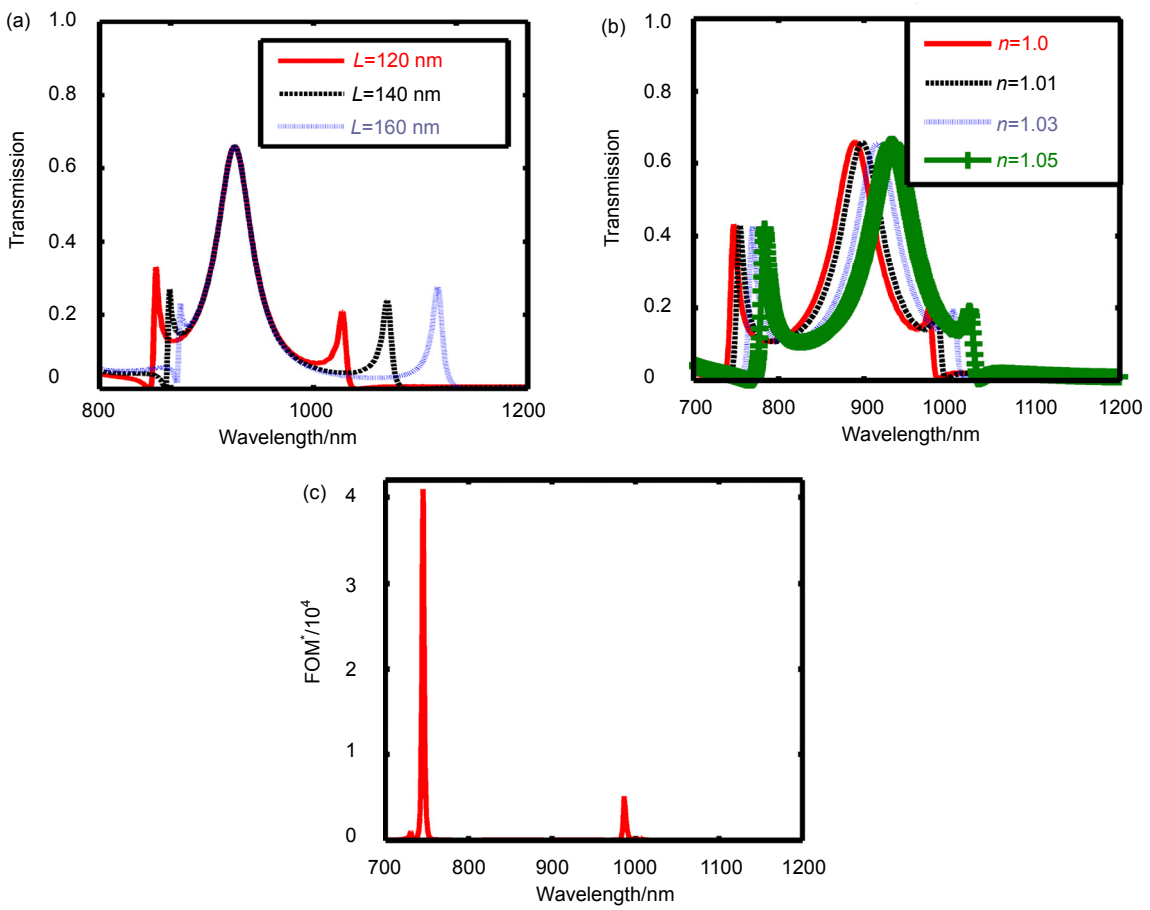

Fig. 6 (a) Fano resonance spectra with L=120, 140 and 160 nm. (b) Fano resonance spectra with L=100 nm and n=1.0, 1.01, 1.03 and 1.05. (c) FOM* variation with respect to wavelength.

References

1 Barnes W L, Dereux A, Ebbesen T W. Surface plasmon subwavelength optics[J]. *Nature*, 2003, **424**(6950): 824–830.

2 Bozhevolnyi S I, Volkov V S, Devaux E, *et al*. Channel plasmon-polariton guiding by subwavelength metal grooves[J]. *Physical Review Letters*, 2005, **95**(4): 046802.

3 Luo Xiangang, Yan Lianshan. Surface plasmon polaritons and its applications[J]. *IEEE Photonics Journal*, 2012, **4**(2): 590–595.

4 Pu Mingbo, Li Xiong, Ma Xiaoliang, *et al*. Catenary optics for achromatic generation of perfect optical angular momentum[J]. *Science Advance*, 2015, **1**(9): e1500396.

5 Wen Kunhua, Hu Yihua, Chen Li, *et al*. Design of an optical power and wavelength splitter based on subwavelength waveguides[J]. *Journal of Lightwave Technology*, 2014, **32**(17): 3020–3026.

6 Zhang Zhao, Shi Fenghua, Chen Yihang. Tunable multichannel plasmonic filter based on coupling-induced mode splitting[J]. *Plasmonics*, 2015, **10**(1): 139–144.

7 Gao Hongtao, Shi Haofei, Wang Changtao, *et al*. Surface plasmon polariton propagation and combination in Y-shaped metallic channels[J]. *Optics Express*, 2005, **13**(26): 10795–10800.

8 Lee T W, Gray S K. Subwavelength light bending by metal slit structures[J]. *Optics Express*, 2005, **13**(24): 9652–9659.

9 Wahsheh R A, Lu Zhaolin, Abushagur M A G. Nanoplasmonic couplers and splitters[J]. *Optics Express*, 2009, **17**(21): 19033–19040.

10 Wen Kunhua, Yan Lianshan, Pan Wei, *et al*. A four-port plasmonic quasi-circulator based on metal-insulator-metal waveguides[J]. *Optics Express*, 2012, **20**(27): 28025–28032.

11 Bavil M A, Zhou Zhipping, Deng Qingzhong. Active unidirectional propagation of surface plasmons at subwavelength slits[J]. *Optics Express*, 2013, **21**(14): 17066–17076.

12 Hu Feifei, Yi Huaxiang, Zhou Zhiping. Wavelength demultiplexing structure based on arrayed plasmonic slot cavities[J]. *Optics Letters*, 2011, **36**(8): 1500–1502.

13 Zou Xihua, Lu Bing, Pan Wei, *et al*. Photonics for microwave measurements[J]. *Laser & Photonics Review*, 2016, **10**(5): 711–734.

14 Zou Xihua, Liu Xinkai, Li Wangzhe, *et al*. Optoelectronic oscillators (OEOs) to sensing, measurement, and detection[J]. *IEEE Journal of Quantum Electronics*, 2016, **52**(1): 0601116.

15 Pannipitiya A, Rukhlenko I D, Premaratne M, *et al*. Improved transmission model for metal-dielectric-metal plasmonic waveguides with stub structure[J]. *Optics Express*, 2010, **18**(6): 6191–6204.

16 Tao Jin, Huang Xuguang, Lin Xianshi, *et al*. A narrow-band subwavelength plasmonic waveguide filter with asymmetrical multiple-teeth-shaped structure[J]. *Optics Express*, 2009, **17**(16): 13989–13994.

17 Han Zhanghua, Forsberg E, He Sailing. Surface plasmon bragg gratings formed in metal-insulator-metal waveguides[J]. *IEEE Photonics Technology Letters*, 2007, **19**(2): 91–93.

18 Wang Bing, Wang Guoping. Plasmon bragg reflectors and nanocavities on flat metallic surfaces[J]. *Applied Physics Letters*, 2005, **87**(1): 013107.

19 Luo Xin, Zou Xihua, Li Xiaofei, *et al*. High-uniformity multichannel plasmonic filter using linearly lengthened insulators in metal–insulator–metal waveguide[J]. *Optics Letters*, 2013, **38**(9): 1585–1587.

20 Xiao Sanshui, Liu Liu, Qiu Min. Resonator channel drop filters in a plasmon-polaritons metal[J]. *Optics Express*, 2006, **14**(7): 2932–2937.

21 Liu Ye, Zhou Fei, Yao Bo, *et al*. High-extinction-ratio and low-insertion-loss Plasmonic Filter with Coherent Coupled Nano-cavity Array in a MIM Waveguide[J]. *Plasmonics*, 2013, **8**(2):1035–1041.

22 Lu Hua, Liu Xueming, Wang Guoxi, *et al*. Tunable high-channel-count bandpass plasmonic filters based on an analogue of electromagnetically induced transparency[J]. *Nanotechnology*, 2012, **23**(44): 444003.

23 Wu Yaw-Dong. High transmission efficiency wavelength division multiplexer based on metal–insulator–metal plasmonic waveguides[J]. *Journal of Lightwave Technology*, 2014, **32**(24): 4242–4246.

24 Zhang Huiyun, Shen Duanlong, Zhang Yuping. Circular split-ring core resonators used in nanoscale metal–insulator–metal band-stop filters[J]. *Laser Physics Letters*, 2014, **11**(11): 115902.

25 Wang Guoxi, Lu Hua, Liu Xueming, *et al*. Tunable multi-channel wavelength demultiplexer based on MIM plasmonic nanodisk resonators at telecommunication regime[J]. *Optics Express*, 2011, **19**(4): 3513–3518.

26 Lu Hua, Liu Xueming, Mao Dong, *et al*. Tunable band-pass plasmonic waveguide filters with nanodisk resonators[J]. *Optics Express*, 2010, **18**(17): 17922–17927.

27 Guo Yinghui, Yan Lianshan, Pan Wei, *et al*. A plasmonic splitter based on slot cavity[J]. *Optics Express*, 2011, **19**(5): 13831–13838.

28 Fano U. Effects of configuration interaction on intensities and phase shifts[J]. *Physical Review*, 1961, **124**(6): 1866–1878.

29 Chen Jianjun, Li Zhi, Zou Yujiao, *et al*. Coupled-resonator-induced fano resonances for plasmonic sensing with ultra-high figure of merits[J]. *Plasmonics*, 2013, **8**(4): 1627–1631.

30 Lu Hua, Liu Xueming, Mao Dong, *et al*. Plasmonic nanosensor based on Fano resonance in waveguide-coupled resonators[J]. *Optics Letters*, 2012, **37**(18): 3780–3782.

31 Wen Kunhua, Hu Yihua, Chen Li, *et al*. Fano resonance with ultra-high figure of merits based on plasmonic metal-insulator-metal waveguide[J]. *Plasmonics*, 2015, **10**(1): 27–32.

32 Wen Kunhua, Hu Yihua, Chen Li, *et al*. Single/dual Fano resonance based on plasmonic metal-dielectric-metal waveguide[J]. *Plasmonics*, 2016, **11**(1): 315–321.

33 Dionne J A, Sweatlock L A, Atwater H A, *et al*. Plasmon slot waveguides: towards chip-scale propagation with subwavelength-scale localization[J]. *Physical Review B*, 2006, **73**(3): 035407.

34 Johnson P B, Christy R W. Optical constants of the noble metals[J]. *Physical Review B*, 1972, **6**(12): 4370–4379.

35 Becker J, Trügler A, Jakab A, *et al*. The optimal aspect ratio of gold nanorods for plasmonic bio-sensing[J]. *Plasmonics*, 2010, **5**(2): 161–167.